Strange quark matter as dark matter: 40 years later, a reappraisal

Francesco Di Clemente [1], Marco Casolino [2], Alessandro Drago [1,3], Massimiliano Lattanzi [1], Claudia Ratti[4]

[1]*INFN, Sezione di Ferrara, via Saragat 1, I-44122 Ferrara, Italy*

[2]*INFN and University of Rome, Tor Vergata, Italy*

[3]*Department of Physics and Earth Science, University of Ferrara, via Saragat 1, I-44122 Ferrara, Italy*

[4]*Department of Physics, University of Houston, Houston, TX 77204, USA*

ABSTRACT

Forty years ago, Witten suggested that dark matter could be composed of macroscopic clusters of strange quark matter. This idea was very popular for several years, but it dropped out of fashion once lattice QCD calculations indicated that the confinement/deconfinement transition, at small baryonic chemical potential, is not first order, which seemed to be a crucial requirement in order to produce large clusters of quarks. Here we revisit both the conditions under which strangelets can be produced in the Early Universe and the many phenomenological implications of their existence. Most of the paper discusses the limits on their mass distribution and a possible and simple scheme for their production. Finally, we discuss the most promising techniques to detect this type of objects.

1 INTRODUCTION

The nature of dark matter remains elusive. One possibility is that dark matter is macroscopic, made of smaller components that can be described within the standard model (Burdin et al. 2015; Jacobs et al. 2015). About forty years ago, it was suggested that dark matter could be made of strangelets, clusters of up, down, and strange quarks (Witten 1984) formed at the time of the QCD phase transition in the Early Universe. The important point is that dark matter made of strangelets can be effectively weakly interacting because it is extremely massive. This possibility is based on the Bodmer-Witten (BW) hypothesis, stating that clusters of strange quark matter (SQM) can be more stable than the most stable atomic nucleus, i.e. ^{56}Fe. The reason why huge amounts of Fe surround us, while we struggle to find any trace of SQM, is that SQM needs a finite and not-too-small fraction of strange quarks in order to be stable. Since multiple, simultaneous weak decays are enormously suppressed, it is clear that the large amount of strangeness needed to satisfy the BW hypothesis can be obtained only under very specific conditions. To date, the only situations in which those conditions can be satisfied are the Early Universe and the core of massive stellar objects.

It is important to note that the validity of the BW hypothesis does not imply that dark matter is made of SQM: it is possible that the hadronization process in the Early Universe does not allow the production of the large clusters of SQM that would constitute dark matter (the possibility that dark matter is made of small clusters of SQM is probably ruled out by observations, as we will discuss in the following). Still, the BW hypothesis could be true, and strange quark stars (QSs) made entirely of SQM could exist (Haensel et al. 1986), since the mechanism of production of SQM in compact stars (which is based on the large chemical potential reached in those objects) is completely different from the one in the Early Universe. On the other hand, if dark matter is indeed composed of SQM, it is very unlikely that QSs do not exist, because many concrete astrophysical paths would lead to their production. This would still not imply that all compact stars are QSs! It is possible to show that, at least in the areas of the galaxies where dark matter is not so abundant, neutron stars (NSs) can exist without being transformed into QSs. This is

of paramount importance, since it is unlikely that all compact stars are QSs and that NSs do not exist, see e.g. Watts & Reddy (2007). Indeed, in the last ten years, a scheme in which NSs and QSs coexist has been developed, the so-called two-family scenario (Drago et al. 2014a,b, 2016; Drago & Pagliara 2016; Wiktorowicz et al. 2017). In that scenario, the most massive objects are QSs; instead, NSs can have small radii, but their maximum mass does not reach 2M$_\odot$.

The very first studies on the equation of state (EoS) of quark matter in compact stars were, in general, based on the MIT bag model (Chodos et al. 1974) and discussed strangeness production (Freedman & McLerran 1978). Three major developments took place after those first pioneering works. 1) Chiral models became popular, based on many variations of the Nambu-Jona Lasinio model (Buballa 2005); 2) Color superconductivity was (re-)discovered. In particular, it has been shown that a phase based on gaps involving color and all three flavors, called Color-Flavor Locked (CFL) phase, could be the absolute ground state of matter, at least at very large densities (Alford et al. 2008). Some of the calculations were based on MIT-bag-like models, but most were based on extensions of chiral models. In the latter, the large mass of the strange quark makes its production difficult even at the center of the most massive compact stars (Buballa 2005; Alford et al. 2008); 3) High order perturbative calculations of dense quark matter were performed, also incorporating strange quarks and stressing that SQM is not soft and it allows for having compact stars with masses largely exceeding 2M$_\odot$ (Alford et al. 2008; Kurkela et al. 2010).

What is the theoretical status of the EoSs that can support the BW hypothesis? While it has been known for many years that MIT-bag-like models can satisfy the requests at the basis of that hypothesis (Farhi & Jaffe 1984), it has been shown that NJL-like models are incompatible with it (Klahn & Fischer 2015). At the moment, it has been demonstrated that the BW hypothesis can also be realized in the color-dielectric model (Drago & Lavagno 2001; Alberico et al. 2002; Dondi et al. 2017) and, more generally, in models in which quark masses have a strong density dependence related to confinement. The BW hypothesis can also be realized in models based on perturbative expansions (Kurkela et al. 2010).

In 1984, when Witten wrote his seminal paper, it was considered very plausible that the primordial confinement/deconfinement phase transition was first order. Lattice QCD calculations have later investigated the order of the phase transition in the regime of small baryonic and leptonic chemical potentials, and it has been found that it corresponds to a smooth crossover (Aoki et al. 2006). Recently it has been shown that, if large leptonic asymmetries are taken into account (which is not excluded by cosmology), the transition can indeed be first order (Gao & Oldengott 2022). It is not yet clear if this will open again the possibility of forming strangelets in the Early Universe following the scheme outlined by Witten. Finally, an important consequence of a first order phase transition in the Early Universe is the production of gravitational waves (Witten 1984) which could contribute to the signal recently detected by the NANOGrav collaboration (Afzal et al. 2023).

Moreover, at LHC experiments such as ALICE, observations have been made of the formation of light nuclei and hypernuclei during proton-proton and nucleus-nucleus collisions (Adam et al. 2016; Braun-Munzinger & Dönigus 2019), even though the temperature at the freeze-out is significantly larger than the scale of their binding energy. This rather surprising result indicates that the process of clusterization can start at those large temperatures and that this process can exist even in the absence of a first-order phase transition. Actually, the process might be based on percolation (Martens et al. 2006), a transition that is, in general, second order (Christensen & Moloney 2005). It has been found that correlations are present between hadrons at temperatures close to the critical one (Bellwied et al. 2021), which might suggest that clusterization can indeed start, maybe using the formation of the H dibaryon (Jaffe 1977) (or sexaquark (Farrar 2022; Shahrbaf et al. 2022)) as the doorway towards the formation of larger clusters. Besides, there are indications that the transition temperature might be flavor-dependent, with strange quarks hadronizing at higher temperatures, compared to light ones (Bellwied et al. 2013; Alba et al. 2020; Flor et al. 2021). This might lead to the early formation of strange clusters in the Early Universe. In conclusion, even if a first order confinement phase transition does not take place in the Early Universe, it is possible that cosmological strangelets can form following mechanisms similar to the ones responsible for the formation of nuclei in ALICE.

In this paper we will shortly revisit the limits on strangelets coming from a variety of astrophysical, cosmological and laboratory observations. We will then produce a set of mass distributions for strangelets, based on a simple scheme similar to the one discussed by Witten (1984) and including the partial evaporation of strangelets as discussed by Alcock & Farhi (1985) and revisited by Madsen et al. (1986). We will fix the few parameters of the model to satisfy all the constraints mentioned above. While this mechanism is not necessarily the correct one, our purpose is to show that it is possible to obtain mass distributions of strangelets that do not violate any observational limit, and based on a simple hadronization scheme.

If a credible distribution of the strangelet masses is obtained, it is possible to estimate their capture rates on the main sequence and on compact stars. Recently, some of us started exploring this idea in connection with possible processes leading to the formation of compact objects having masses of the order of or smaller than one solar mass (Di Clemente et al. 2022; Di Clemente et al. 2023), as suggested in Di Salvo et al. (2019) and in Doroshenko et al. (2022), The possible implications of a dark matter made of SQM on the stellar evolution are certainly much broader and will require more extensive analyses.

Another problem that can be tackled once a candidate distribution of strangelets is at hand, is the formation of supermassive black holes.

It has been suggested that self-interacting dark matter can form black hole seeds in the center of a halo, potentially solving the problem (Pollack et al. 2015). We will show that strangelets do not satisfy the requests on self-interaction needed to solve that problem, but on the other hand they interact with ordinary matter and the implications of that interaction still need to be explored.

Finally, if the mass distribution of strangelets is obtained, it is possible to formulate well-focused campaigns to search for these objects. In the last part of this manuscript, we discuss possible search strategies to find the strangelets with the mass distribution that we predict.

2 OBSERVATIONAL CONSTRAINTS

Dark matter could be either intrinsically weakly interacting, or effectively weakly interacting due to its large mass and, consequently, its low number density (Jacobs et al. 2015). The primary candidates for dark matter have been for a long time Weakly Interacting Massive Particles (WIMPs), but the lack of conclusive evidence from collider experiments and from campaigns of direct detection has left their existence uncertain.

Strangelets belong to the macros category, which has to respect several observational constraints from different sources (Jacobs et al. 2015; Burdin et al. 2015). The mass ranges not subject to limits for nuclear density monochromatic macros in the present Universe are $(55 - 10^3)$ g, $(5 \times 10^4 - 10^8)$ g and $(10^{10} - 10^{18})$ g (Singh Sidhu & Starkman 2020; Burdin et al. 2015). In the case of strangelets, other constraints must also be taken into account, because they can interact with ordinary matter, dramatically altering the astrophysical evolution of stars. In particular, Madsen (1988) rules out the two lowest mass windows, leaving open (at least for monochromatic strangelets) only the range $(10^{10} - 10^{18})$ g.

Here follows a short list of the main current observational constraints.

2.1 Ancient Mica

Strangelets with low enough mass, would have a high enough number density to have left a record on Earth. If the mass was not very large, they could have penetrated a few kilometers into the Earth's crust, thus leaving an imprint into ancient muscovite mica. In examining the potential impact of macros on ancient mica, the study of Jacobs et al. (2015) accounts for the absence of traces found in the sample considered by Price & Salamon (1986) and it excludes strangelets having a mass $M < 55$ g.

2.2 Seismic events

Limits on the mass have been set by considering seismic events on Earth and on the Moon (Burdin et al. 2015; Herrin et al. 2006). Concerning seismic events on Earth, the mass range 10^5 g $< M < 3 \times 10^8$ g as dominant dark matter component can be excluded. Moreover, from the measurements of the total amount of seismic energy, estimated by using the seismic station on the Moon implanted during the Apollo missions, it is possible to conclude that less than 10% of dark matter density is in the mass range 5×10^4 g $< M < 10^6$ g.

2.3 Femtolensing

One of the ways to search for compact astrophysical objects that could constitute dark matter, is through the lensing effects that they would

cause. Femtolensing is an interference effect in the energy spectrum of the lensed object. Using Fermi satellite data, Barnacka et al. (2012) have set a limit of contribution to dark matter mass of 8%, for compact objects having masses in the range of 5×10^{17} g $< M < 2 \times 10^{20}$ g. Nevertheless, the more recent analysis from Katz et al. (2018) which revised femtolensing, states that there is no such a limit.

2.4 Microlensing

The analysis of Singh Sidhu & Starkman (2020) rules out macros in the range of mass 5×10^{22} g $< M < 4 \times 10^{24}$ g as the dominant component of dark matter. Moreover, Jacobs et al. (2015) rules out macros having $M \geq 10^{24}$ g.

2.5 Thermonuclear runaway

A macro of sufficiently large cross-section impacting a white dwarf (WD) or a neutron star would release an energy leading to a thermonuclear runaway, therefore a supernova explosion. Based on this assumption, the Singh Sidhu & Starkman (2020) analysis excludes the mass ranges 10^8g $< M < 10^{10}$g and $M > 10^{18}$ g for nuclear density macros.

2.6 Proto-neutron stars

Not all compact stars are QSs (Watts & Reddy 2007). A strangelet can penetrate a newly formed NS, before a crust forms, and convert it into a QS. Therefore, one needs to impose a limit on the strangelet flux. Given τ_{melt} as the time before the NS forms a crust able to stop strangelets (Madsen 1988) and given that only strangelets with a baryon number $A > 10^{12}$ can evade being trapped by the expanding supernova shell, the relation $F_{12} \times \tau_{\text{melt}} \ll 1$ must hold, where F_{12} is the flux of strangelets having $A > 10^{12}$.

3 A SIMPLE PHENOMENOLOGICAL MODEL

In the following, we discuss a model for the production of strangelets in the Early Universe, based on the scheme developed in Witten (1984), and incorporating the evaporation mechanism discussed in Alcock & Farhi (1985) and revisited by Madsen et al. (1986). This simple scheme does not discuss many relevant problems which emerged during the forty years after the publication of the paper of Witten (1984). In particular, the mechanism of chiral symmetry breaking was not incorporated in that scheme, which was loosely modeled on the MIT bag model. In Farhi & Jaffe (1984), they discussed values of the bag constant B, of the strong coupling α_s and of the strange quark mass m_s for which SQM is absolutely stable, but most of that parameter space has now been ruled out, in particular by analyses of heavy ion collisions. On the other hand, the study of the formation of gapped phases has shown that absolutely stable SQM can be obtained in a CFL phase (Alford et al. 2008).

While in the following we discuss a simple scheme, still based on the papers of Witten (1984) and Alcock & Farhi (1985), at the end of this section we will propose a possible path for the Early Universe which is compatible with recent microphysics and still leads to the formation of cosmological strangelets.

3.1 Evaporation

Witten (1984) discusses the typical size of cosmological strangelets, formed at the time of hadronization, suggesting that it could be of the order of centimeters. As discussed above, that analysis needs to be revisited, and we will simply assume that the initial size of the strangelets is regulated by a distribution, that we choose to be log-normal, as suggested by studies on the coalescence of droplets (Davis & Smith 1973). A log-normal distribution has also been used to describe the sizes of coalescing primordial black holes (Dolgov et al. 2020). This distribution will be modified by the process of evaporation.

The evaporation of SQM, as discussed by Alcock & Farhi (1985), is a crucial phenomenon to understand the behavior of matter in the Early Universe. In particular, when the Universe cools from $T \sim 150$ MeV to $T \sim 1$ MeV, the evaporation of SQM plays an important role in determining the survival and stability of strangelets.

The stability of strangelets is highly dependent on their baryon number. Alcock & Farhi (1985) suggest that strangelets, with a baryon number smaller than a critical one, evaporate completely in the Early Universe. Notice anyway that strangelets having a baryon number larger than the critical one undergo only a partial evaporation, and the final distribution of their sizes is therefore the result of this process.

The mechanism of evaporation primarily involves the emission of nucleons from the strangelet. This process is regulated by various mechanisms, described in the following as outlined in Alcock & Farhi (1985), in particular: the thermal balance of the strangelet which cools down by the evaporation process itself and needs to be kept warm by neutrinos; the net-rate of emission of nucleons by an isolated strangelet; the increase in the re-absorption rate due to the presence of evaporated nucleons close to the surface of the strangelet; the opacity of the evaporated material to neutrinos. In more details:

- the primary consideration is the energy balance, which includes the cooling effects due to evaporation and neutrino emission, and the reheating effects from incoming neutrinos. The probability of neutrino absorption is contingent on the neutrino's mean free path $l(T)$, the strangelet size r_s ($\propto A^{1/3}$), and the environment temperature T. If the size of the lump exceeds the mean free path of a neutrino, it becomes opaque to neutrinos and will emit them with a thermal spectrum. The energy emission rate of strangelets, determined by its surface temperature T_s, is given by:

$$L_{\text{th}} = 4\pi r_s^2 (7\pi^2/160) T_s^4 \tag{1}$$

indicating that the lump radiates according to its temperature T_s. On the other hand the absorption rate reads:

$$L_{\text{abs}} = 4\pi r_s^2 (7\pi^2/160) T_u^4, \tag{2}$$

where T_u is the temperature of the Universe. For a strangelet smaller than the neutrino mean free path, the emission and the absorption rates should be adjusted by incorporating a probability factor:

$$p(r_s, T) = \begin{cases} 1, & r_s > \frac{3}{4} l(T) \\ \frac{4 r_s}{3 l(T)}, & r_s \leq \frac{3}{4} l(T). \end{cases} \tag{3}$$

Therefore, the total rate reads:

$$L = 4\pi r_s^2 \left(\frac{7\pi^2}{160}\right) \left[T_u^4 \, p(r_s, T_u) - T_s^4 \, p(r_s, T_s) \right]. \tag{4}$$

- By solving a detailed balance equation, it is possible to estimate the net emission rate of nucleons from an isolated strangelet:

$$r_{n,p} = \frac{m_N T_s^2}{2\pi^2} e^{-I/T_s} f_{n,p} \, \sigma_0 A^{2/3}, \tag{5}$$

where f_n (f_p) are the neutron (proton) absorption efficiencies, I is the binding energy, $\sigma_0 A^{2/3}$ is the geometrical cross section and $\sigma_0 = 3.1 \times 10^{-4}$ MeV^{-2} is obtained by assuming a density of $(125$ MeV$)^3$, while m_N is the nucleon mass.

• It is necessary to consider that nucleons close to the surface of strangelets might be reabsorbed [1]. The rates at which neutrons and protons are reabsorbed are as follows:

$$r_{n,p}^{\text{abs}} = f_{n,p} N_{n,p} \sigma_0 A^{2/3} (T_s/2\pi m_N)^{1/2} \tag{6}$$

where N_n (N_p) are the neutron (proton) densities, which depend on the temperature.

• Local densities of neutrons and protons are determined by pressure equilibrium. We take into account the contribution of electrons, positrons, photons, nucleons, and the contribution of neutrinos since we assume that they interact with the evaporated material:

$$\left(N_n + N_p\right) T + \frac{43\pi^2}{360} T^4 = \frac{43\pi^2}{360} T_u^4. \tag{7}$$

Including all emission and absorption terms, the net-evaporation rate of a cosmological strangelet can be formulated as:

$$L = \frac{dA}{dt}\left(I + 2T_s\right), \tag{8}$$

where:

$$\frac{dA}{dt} = \left[\frac{m_N T_s^2}{2\pi^2} e^{-I/T_s} - \frac{43\pi^2}{720T_s}\left(T_u^4 - T_s^4\right)\left[\frac{T_s}{2\pi m_N}\right]^{1/2}\right] \\ \times \sigma_0 A^{2/3}\left(f_n + f_p\right). \tag{9}$$

Note that dA/dt is the evaporation rate, a positive quantity, and it has the opposite sign with respect to the rate of change of the baryon content of the strangelet. By combining Eq. 4, Eq. 8, and Eq. 9 one can obtain an equation relating T_u, T_s and A:

$$\frac{k_1 \left[T_u^4 p\left(T_u, A\left(T_u\right)\right) - T_s^4 p\left(T_s, A\left(T_u\right)\right)\right]}{\left(2T_s + I\right)\left(f_n + f_p\right)} \\ = -\frac{k_2 \left(T_u^4 - T_s^4\right)}{\sqrt{T_s}} + \frac{m_N T_s^2 e^{-\frac{I}{T_s}}}{2\pi^2}. \tag{10}$$

• The evaporated material surrounding the strangelets can be thick to neutrinos. At high temperatures, neutrinos are absorbed by that external layer and cannot reach the strangelets. In that situation, evaporation is suppressed. This limiting temperature T_{evap} is indicated in Fig. 1 of Alcock & Farhi (1985), it depends on the mass of the strangelet and it is in the range $50\,\text{MeV} \lesssim T_{\text{evap}} \lesssim 120\,\text{MeV}$. We will consider T_{evap} as a free parameter.
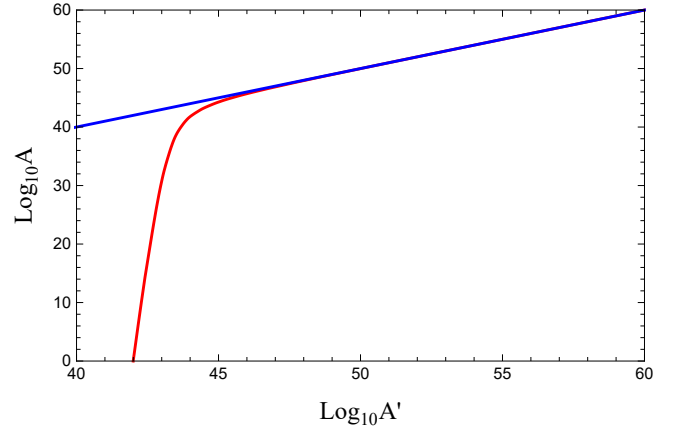
Finally, given the relationship between the age of the universe τ_U and its temperature T_u in the radiation-dominated era (Alcock & Farhi 1985):

$$\tau_U = \left(\frac{45}{172\pi^3 G}\right)^{1/2} \frac{1}{T_u^2}, \tag{11}$$

it is possible to write the evaporation rate as a function of the temperature T_u alone:

$$\frac{dA}{dT_u} = -\frac{\left(\beta k_3 A^{2/3}\left[T_u^4 p\left(T_u, A\right) - T_s^4 p\left(T_s, A\right)\right]\right)}{\left(2T_s + I\right) T_u^3}. \tag{12}$$

---

[1] At the high temperatures relevant for evaporation the Coulomb barrier surrounding the strangelets does not stop the protons from being absorbed, see discussion in subsection 3.3

Figure 1. Red curve: example of the function $A = f(A')$, which maps A', the size of the strangelets pre-evaporation, onto the post-evaporation size A. In this example, strangelets having $A' \lesssim 10^{42}$ evaporate completely. It is compared with the blue curve, which corresponds to the case in which there is no evaporation.

Here and in Eq. 10, k_1, k_2 and k_3 are parameters that incorporate various physical constants into the model. Additionally, we introduce a phenomenological factor β to account for corrections related to Pauli blocking, to the finite value of the strange quark mass and to QCD effects. These corrections can suppress the evaporation rate by several orders of magnitude (Madsen et al. 1986; Madsen 1988). By solving Eq. 10 and Eq. 12, one can effectively determine the dynamics of strangelet evaporation during the cooling phase that follows hadronization.

3.2 Strangelet distributions

To accurately model the current distribution of dark matter in the galaxy as strangelets, one must consider various factors, including the strangelet size distribution. Initially, we hypothesize a log-normal distribution of sizes and then subject it to an evaporation process. This evaporation, occurring in a range of temperatures from 150 MeV to 1 MeV, results in a transformed distribution that must agree with the constraints specified in Section 2.

3.2.1 Mathematical framework

It is crucial to establish a mathematical framework for handling the size distributions of strangelets. Here we will follow the scheme deveoped in Bucciantini et al. (2022). Given an initial distribution $P(A')$, representing the number of strangelets with a baryon number A', the distribution after evaporation, denoted as $Q(A)$, is given by:
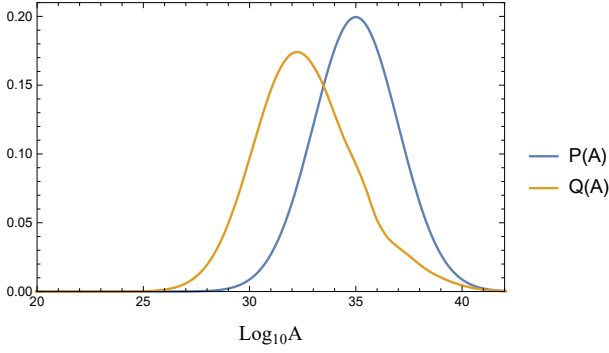
$$Q(A) = \int_1^\infty dA' P(A')\delta(A - f(A')). \tag{13}$$

Here, $f(A')$ is the function that maps the pre-evaporation baryon number A' onto the post-evaporation baryon number A, see Fig. 1, and it can be evaluated by using the technique outlined in the previous section.

It is important to remark that the number of strangelets is not conserved during the process of evaporation, since those having a size smaller than a critical one evaporate completely:

$$\int_1^\infty Q(A)\, dA < \int_1^\infty P(A)\, dA \tag{14}$$

Figure 2. Example of the relation between the pre-evaporation distribution $P(A)$ and the final distribution $Q(A)$. $P(A)$ is a log-normal distribution with $\mu_{\max} = 35$, $\sigma = 2$. $Q(A)$ is obtained by evaporation, by assuming $\log_{10} \beta = -4.7$ (see Eq. 12). Here $P(A)$ is normalized to 1.

This framework allows us to map the initial distribution of the baryon number of strangelets onto the distribution after evaporation. In this way, the total amount of baryons, evaporated from the strangelets, will provide the baryon number of ordinary matter, allowing us to achieve consistency with observational constraints.

3.2.2 Parameters of the model

As discussed above, we assume that the initial number distribution of strangelets having a given mass, at the time of hadronization and before evaporation, is log-normal. It reads:
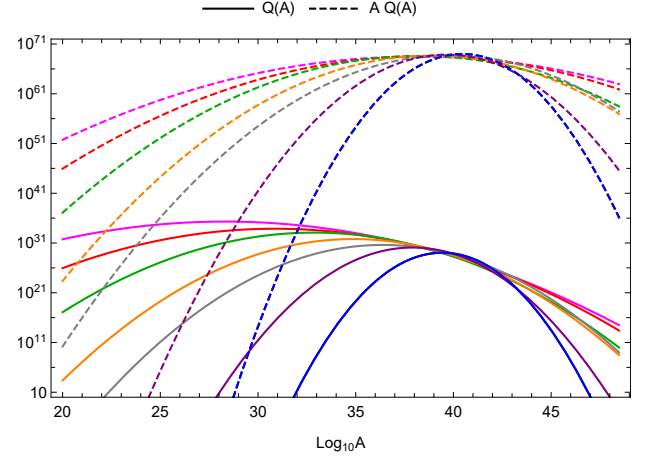
$$f(A; \mu, \sigma) = \frac{1}{A\sigma\sqrt{2\pi}} \exp\left(-\frac{(\ln A - \mu)^2}{2\sigma^2}\right), \tag{15}$$

where μ and σ are the mean and the standard deviation of the variable's logarithm, not of the variable A itself. Notice that the maximum of the log-normal is located at $\ln A = \mu - \sigma^2 \equiv \mu_{\max}$. In Fig. 2 we show an example of the initial distribution $P(A)$ and of the post-evaporation distribution $Q(A)$.

In our scheme we have therefore four parameters regulating the final distribution $Q(A)$: the mean μ and the standard deviation σ of the log-normal distribution; the temperature T_{evap} at which neutrinos can reheat the strangelets and evaporation becomes efficient; the parameter β, regulating the evaporation rate.

To evaluate the viability of this model, several constraints must be considered. These include ensuring that the final distribution aligns with the observed ratio of dark matter in the Milky Way, which is approximately 90% of the total matter content (Watkins et al. 2019). Additionally, the model must adhere to the observational constraints outlined in Section 2. Through a systematic exploration of the parameter space, we correlate the initial distribution parameters with those of the final distribution. This approach enables us to control and predict key characteristics of the strangelet population, including the maximum of the final distribution of the baryon number $Q(A)$ and of the mass $AQ(A)$, and the final number of strangelets $N \equiv \int Q(A)\mathrm{d}A$.

In Appendix A we analyze the impact of these four parameters on the final distribution of strangelets. An important outcome of that analysis is that, if we reduce the value of T_{evap} i.e. if we assume that evaporation starts being effective at lower temperatures, we get final distributions similar to the ones obtained by reducing the value of β, i.e. assuming a strong suppression of the decay rate. In particular, we get similar results if we assume $T_{\text{evap}} \sim 150\text{MeV}$, $\beta \sim 10^{-5.6}$

Figure 3. This figure showcases distributions with varying number densities and mass densities of strangelets. The represented curves, in red, green, yellow, grey, purple, and blue, correspond to distributions containing approximately 10^{34}, 10^{33}, 10^{32}, 10^{31}, 10^{30}, and 10^{29} strangelets, respectively. Notably each curve, despite having different peak densities, has the same total mass. Furthermore, each distribution agrees with the femtolensing observational constraints and other relevant ones as detailed in Singh Sidhu & Starkman (2020) and Burdin et al. (2015). The distributions are normalized to the estimated dark matter mass in the Milky Way (Nesti & Salucci 2013).

or if instead we use $T_{\text{evap}} \sim 50\text{MeV}$, $\beta \sim 10^{-4}$. This second choice is probably more realistic in light of the analyses of Alcock & Farhi (1985) and of Madsen et al. (1986); Madsen (1988).

3.2.3 Galactic distribution

By implementing the evaporation model on the initial distributions $P(x)$, and ensuring the agreement with the constraints, we have been able to calculate the number distribution of strangelets and the mass distribution. These distributions are plotted in Fig. 3.
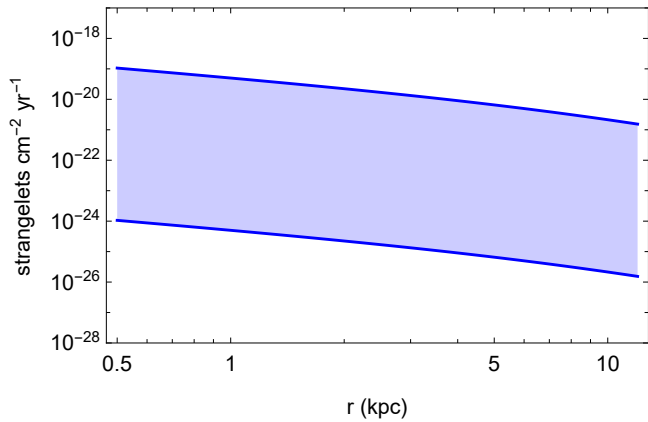
Understanding the astrophysical implications of dark matter, particularly if a portion of it is composed of strangelets, necessitates an estimation of the flux of strangelets impacting on celestial bodies. For this purpose, we utilize the NFW profile (Navarro et al. 1997), which is a well-established model in astrophysics, widely used for describing the density distribution of dark matter in galaxies. As described in Nesti & Salucci (2013), the NFW profile is given by

$$\rho_{NFW} = \rho_H \frac{1}{x(1+x)^2}, \tag{16}$$

where ρ_H represents the characteristic density scale of the profile. The dimensionless variable x is defined as $x = r/R_H$, with R_H being a scale radius. The profile's slope at R_H is characterized by:

$$\left[\frac{d\log\rho_{NFW}}{d\log r}\right]_{r=R_H} = -2. \tag{17}$$

Utilizing the parameters estimated by Nesti & Salucci (2013), we can calculate the expected flux of strangelets as a function of the distance from the center of the Milky Way. This calculation is crucial in understanding the spatial distribution and potential impact of strangelets. The results are illustrated in Fig. 4. Despite its simplicity, this analysis is key in evaluating the feasibility of strangelets as dark matter candidates and their potential observable signatures.
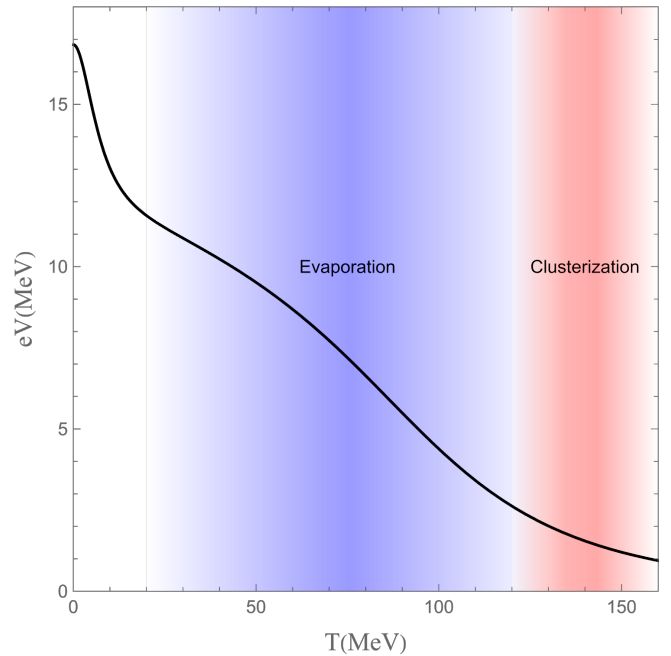
Figure 4. The plot illustrates the expected flux of strangelets, with the number of strangelets ranging from 10^{29} to 10^{34} (see Fig. 3), as a function of the distance from the Galactic center.

3.3 Rephrasing Witten with a modern language

As already discussed, some of the hypotheses assumed in Witten (1984) and Farhi & Jaffe (1984) are probably not compatible with what is now known about microphysics. In particular the following questions were not discussed, mostly because forty years ago these problems were still in a very primordial stage or completely unknown: chiral dynamics across the critical temperature; compatibility of the value of the bag pressure with the results of experiments of heavy ion collisions; role played by the formation of diquark condensates. In this section we discuss a possible path, incorporating state-of-the-art knowledge of quark dynamics which, although speculative, could lead to the formation of strangelets in a way which is phenomenologically not too different from the one based on the papers of Witten (1984) and Farhi & Jaffe (1984). It is indeed interesting to remark that the distribution of the size of the strangelets, obtained in the previous section by taking into account all observational limits, peaks at sizes very close to the one estimated in the paper by Witten (1984). It is therefore important to investigate whether a cosmological path, incorporating up-to-date results of microphysics, can still support that result.

We propose a scheme based on the following stages:

• lattice QCD simulations show that, at temperatures larger than the critical one, strong correlations between quarks can take place (Bellwied et al. 2021). If the cosmological trajectory is not too far from the critical end point (Gao & Oldengott 2022), these correlations can correspond to the formation of pre-clusters, as discussed in Shuryak & Torres-Rincon (2020). Notice that, at this stage, chiral symmetry is still restored and therefore the masses of up, down and strange quarks are still small;

• while the transition is not assumed to be first order, we imagine that the decrease of the temperature can lead to an increase of the correlations and to the gradual development of binding energy in the cluster. Once the (pre-)cluster is bound, its total energy can be described by a semi-empirical mass formula, including also a surface term. While this step is still speculative, the formation of nuclei in heavy ion collisions (Adam et al. 2016; Braun-Munzinger & Dönigus 2019) supports this hypothesis since it shows that the formation of bound clusters can take place even if a first order phase transition is not observed;

• the size of clusters can dramatically increase, by a process of coalescence totally similar to the one discussed by Witten (1984). In

Figure 5. Coulomb barrier for a particle of unitary charge e as a function of the temperature T. The calculation has been performed by using the MIT bag model, setting the bag constant to $B = 145^4$ MeV^4 and with quark masses: $m_{up} = 1$ MeV, $m_{down} = 1$ MeV, $m_{strange} = 150$ MeV.

this way, the initial distribution of the size of the strangelets should peak in the same range indicated by Witten (1984);

• when the temperature further decreases, chiral symmetry breaks. The quark masses increase, including the mass of the strange quark, and the cluster becomes meta-stable. The presence of a surface energy implies that the clusters are not immediately destroyed. The process of evaporation is also suppressed because neutrinos (crucial to evaporation, as discussed in the previous section) are absorbed by the layer of evaporated hadrons and they are therefore unable to keep the cluster hot (Alcock & Farhi 1985);

• since up, down and strange quarks are already present in the cluster, nothing stops the cluster from increasing its density in order to minimize its energy by forming a phase in which quarks are gapped. At that point, the clusters are totally stable and they follow the partial evaporation path described in the previous section. Notice that once clusters form, large enough to be described through hydrodynamics, the process of conversion from normal quark matter to gapped quark matter is very rapid, due to the onset of hydrodynamical instabilities (Drago et al. 2007). This mechanism of stabilizing clusters of SQM has been addressed in several papers, including the ones discussing the evolution of an entire strange quark star Alford & Reddy (2003); Drago et al. (2004).

A macroscopic isolated strangelet develops a Coulomb barrier, similarly to what happens in the case of a strange quark star (Alcock et al. 1986). The height of the barrier depends on the temperature (Kettner et al. 1995) and in Fig. 5 we show this dependence. At low temperatures ($T \lesssim 1$MeV) the barrier is large enough to stop the absorption of protons. Instead, for $T \sim$ a few ten MeV (the range relevant for evaporation), the barrier is already low compared to the temperature and therefore it can be neglected when discussing proton re-absorption (see subsection 3.1). Finally, for $T \gtrsim 100$ MeV at which clusterization still takes place, the Coulomb barrier has not

yet formed and the value indicated in Fig. 5 corresponds just to an upper limit.

Of course the scheme discussed above is speculative and detailed analyses will be needed in order to clarify all the steps. For instance, it is crucial to understand the evolution of the (pre-)clusters with the temperature. Also, the cosmic trajectory has, up to now, been computed assuming a small contribution of multistrange particles (Letessier & Rafelski 2002). It will be interesting to investigate if some of the models used to describe the formation of nuclei at high temperature, as observed in heavy ion collision experiments, can be adapted to the cosmological scenario. Another important point has to do with the formation of gapped quark matter. We do not know if the gapping will directly produce Color-Flavor-Locked quark matter Alford et al. (2008), or if it will form, at least as an intermediate step, a crystalline phase as the one described in Anglani et al. (2014). Notice that the knowledge of which gapping pattern will actually take place is important also for the phenomenology of dark matter, since Color-Flavor-Locked quark matter is totally neutral, while a crystalline phase needs the presence of electrons to achieve charge neutrality.

4 ASTROPHYSICAL IMPLICATIONS

We can study the impact of the possible existence of strangelets by estimating the capture rate onto astrophysical objects as main sequence stars. Madsen (1988) has already discussed the conditions to have interaction or capture of a strangelet by a star. It is expected that a strangelet would pass through a star like the sun without being captured, given its velocity and cross section.

In order to estimate the capture rate from a main sequence star, we use the flux formula from Jacobs et al. (2015), opportunely modified to take into account the strangelet number and distribution:
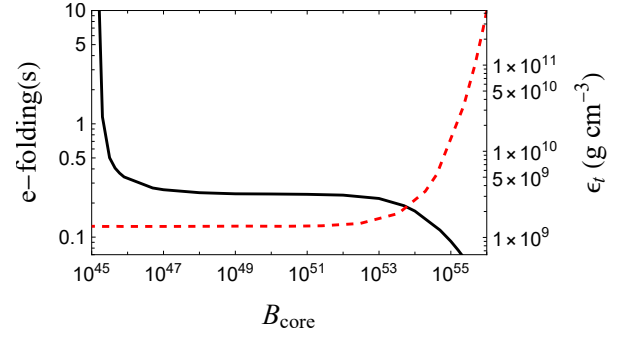
$$
F = 2.7 \times 10^{29} \frac{\rho_{\mathrm{NFW}}(r)}{\rho_{\mathrm{DM}}} \frac{N}{M_{\mathrm{V}}} \frac{M}{\mathrm{M}_\odot} v_{250} \left(\frac{R_c}{\mathrm{R}_\odot} \right)^2
$$
$$
\times \left(1 + 6.2 \left(\frac{\mathrm{R}_\odot}{R_t} \right) v_{250}^{-2} \left(\frac{M_t}{\mathrm{M}_\odot} \right) \right), \quad (18)
$$

where N is the total number of strangelets in the galaxy, M_{V} is the virial mass of the Milky Way in units of the proton mass, v_{250} is the velocity of DM in units of 250 km/s, M is the mass of the star, R_c is the radius of the star core (which is the part of the star capable of stopping strangelets (Madsen 1988)). Indeed, we have extended the formula originally proposed by Jacobs et al. (2015) to account for the fact that only strangelets colliding with the dense central region of a star, characterized by a radius R_c, can be halted, while others may pass through.

To estimate the capture on a star, we have to consider a star which has already formed a core dense enough to stop a strangelet. Indeed, we choose the silicon formation because the mass density would be enough to start stopping some strangelets. Therefore, in order to estimate the capture probability, Eq. 18 has to be multiplied by $\tau(M)$, which is the time interval between the silicon formation in the core of a star having mass M and its collapse.

4.1 Strange Dwarfs

An astrophysical implication of the presence of cosmological strangelets is the impact they can have on the evolutionary path of WDs which, capturing strangelets in their lifetime, become strange

Figure 6. Dependence of the instability timescale on the core size. The solid black line shows the timescale of the mechanical instability as a function of the baryonic content of the core (B_{core}). The dashed red line shows the density of nuclear matter at the interface with the SQM core. Plot from Di Clemente et al. (2023).

dwarfs (SDs). The SD existence and stability have been argued several times (Glendenning et al. 1995a,b; Vartanyan et al. 2009, 2012; Alford et al. 2017; Kurban et al. 2022; Di Clemente et al. 2023).

Glendenning et al. (1995a) analyzed the radial stability of SDs, suggesting they could be stable even for density of nuclear matter exceeding the maximum for regular WDs. However, Alford et al. (2017) challenged this view. They found that the fundamental radial mode eigenvalue was negative, implying instability in such systems. This apparent contradiction is solved in Di Clemente et al. (2023), addressing the study of the boundary conditions (Pereira et al. 2018; Di Clemente et al. 2020) at the interface between nuclear matter and the quark core.

When a WD gets close to Chandrasekhar's mass, large density fluctuations trigger nuclear fusion processes which end up with a supernova explosion. Di Clemente et al. (2023) showed that, if the SQM core is large enough, the timescale of the gravitational collapse becomes much shorter than the timescale of nuclear reactions, leading the WD to a collapse instead of a supernova.

4.2 Central compact object in HESS J1731-347

The study of the central compact object within the supernova remnant HESS J1731-347 indicates a small mass that is potentially subsolar (Doroshenko et al. 2022), namely an estimated mass of $0.77^{+0.20}_{-0.17} \mathrm{M}_\odot$ and a radius $R = 10.4^{+0.86}_{-0.78}$ km. Such attributes pose a conundrum for traditional models of supernova explosions, which typically fail to account for the existence of neutron stars with gravitational masses smaller than $\sim 1.17 \mathrm{M}_\odot$ (Suwa et al. 2018). Hence, this compact object can be assumed to be a strange quark star (Di Clemente et al. 2022).

To form a low-mass strange star, one can account for processes similar to those that result in the formation of light neutron stars. In the notable case of an electron-capture supernova, one has to consider a progenitor, which is a main-sequence star with a mass around $8 \mathrm{M}_\odot$ (Suwa et al. 2018). For the progenitor to evolve into a strange star instead of a neutron star, it must have undergone an

essential precondition: the accumulation of strange matter near its core. This accumulation could occur when, during the evolution of the star, the core is dense enough to stop a strangelet (Madsen 1988). As the progenitor star undergoes the supernova event, the presence of accumulated strangelets favors the conversion of hadronic matter into strange matter, leading to the birth of a strange star with a relatively small mass.

Owing to the larger binding energy of strange quark stars, they can have a lower gravitational mass while having a baryonic mass equivalent to that of the lightest neutron stars ($\sim 1.28 M_\odot$). The strange star, just conserving the baryonic content, will have a mass that oscillates between $0.95 M_\odot$ and $1.08 M_\odot$, instead of a neutron star. It should be noted that the transition from hadronic to strange matter is markedly exothermic. Thus, during the supernova event, it is reasonable to hypothesize that a larger amount of matter is expelled, compared to the process of neutron star formation, thus resulting in the formation of a correspondingly lighter object.

4.3 Solar flares

In the analysis presented by Bertolucci et al. (2017), the correlation between solar phenomena such as flares and Extreme Ultraviolet (EUV) emissions and the heliocentric longitudes of Earth and the inner planets is explored, suggesting a potential link to increased solar activity during specific planetary alignments. This observation corroborates the hypothesis that slow-moving, galactic or cosmic-origin dark matter streams, potentially comprising anti-quark nuggets (a specific strangelets model), could be interacting with the Sun, influenced by the gravitational lensing effects of the planets. The peculiar behavior of these streams might be a significant contributor to various observed solar phenomena.

The study, while focused on a specific model of strangelets as proposed by Zhitnitsky (2003), hints at a broader applicability. The observed correlations could be indicative of a class of dark matter that interacts more strongly than the traditionally considered WIMPs.

The underlying assumption is that this dark matter, regardless of its exact nature, interacts with the solar atmosphere in a way that could trigger increased solar activity. The solar atmosphere acts as a unique detector for these interactions due to its sensitivity to low-energy deposition, a condition not easily replicated with terrestrial dark matter detection methods. The potential for planetary gravitational lensing to focus these dark matter streams onto the Sun, thereby increasing the likelihood of solar flares or other activities, represents a novel approach to understand both solar dynamics and macro dark matter properties.

5 IMPLICATIONS FOR COSMOLOGY

Macroscopic dark matter candidates, like strangelets, exhibit a peculiar phenomenology related to the fact that, differently e.g. from WIMPs, they interact with themselves and with ordinary matter. The effects of these interactions on cosmological observables are typically controlled by the reduced cross section σ/M. In this section, unless otherwise stated, we will assume that SQM makes up for all the dark matter content of the Universe.

Self-interacting dark matter has been proposed as an alternative to alleviate, or altogether eliminate, some shortcomings of the collisionless cold dark matter paradigm at galactic scales (Carlson et al. 1992; Spergel & Steinhardt 2000). Indeed, self-interacting dark matter, with velocity-independent reduced cross-section σ_{self}/M in the range $(0.1 - 1)\, \text{cm}^2\, \text{g}^{-1}$, would solve the core-cusp and "too big to

fail" problems of cold dark matter, while at the same time satisfying constraints from massive galaxy clusters (see Bullock & Boylan-Kolchin (2017) for a review). Notice anyway that the elastic reduced cross section is very small for clusters of SQM having the size discussed in the present paper:

$$\frac{\sigma_{\text{self}}}{M} = \frac{3}{\rho\, r_s} \sim 10^{-14} \left(\frac{r_s}{\text{cm}} \right)^{-1} \text{cm}^2\, \text{g}^{-1} \sim 0.1 A^{-1/3} \text{cm}^2\, \text{g}^{-1}\,,$$

(19)

where we have used the fact that σ_{self} is related to the geometrical cross section σ_{geom} through $\sigma_{\text{self}} = 4\sigma_{\text{geom}} = 4\pi r_s^2$.

Interactions between dark matter particles and baryons generate a drag force that suppresses the growth of cosmic structures at small scales. This can be used to derive constraints on the dark matter-baryon scattering cross section. Dvorkin et al. (2014) consider a velocity-dependent cross section $\sigma_{\text{scatt}} \propto v^n$, with $-4 \leq n \leq 2$. For a velocity-independent cross section, they find $\sigma_{\text{scatt}}/M < 3.3 \times 10^{-3}\, \text{cm}^2\, \text{g}^{-1}$ at 95% CL from a combination of CMB data from Planck and Ly-α data from the Sloan Digital Sky Survey. As in the case of dark matter self-interactions, these constraints are practically irrelevant for the clusters of SQM discussed in this paper.

Even though the elastic reduced cross section of strange matter is small, an open question concerns the inelastic cross section of this type of matter. In Bauswein et al. (2010) it has been shown that the "sticky properties" of strange matter, produced after the merger of two strange quark stars, deeply modify the dynamics of the system, if compared with that of ordinary matter. In particular, they lead to the formation of spiral arms which remain located close to the equatorial plane. The implications of this property for structure formation still need to be worked out. Jacobs et al. (2015) argue that the constraints for inelastic self-interactions should be at least as strong as those for elastic scattering. Thus, in the absence of stronger arguments, one can treat the bounds on the elastic cross section as also being (conservative) bounds on the inelastic cross section. These are anyway automatically respected by SQM satisfying the bounds on the elastic cross section, since the absorption cross section is suppressed by the Coulomb barrier.

The electromagnetic properties of dark matter are also severely constrained by observations. The general argument that we have just sketched, about the drag force generated by dark matter-baryon scatterings, can be specified to the case of electromagnetic interactions. Constraints on the DM charge from Planck 2013 data were first derived by Dolgov et al. (2013). Dvorkin et al. (2014) express these constraints on the scattering cross section in terms of the DM charge ($\sigma_{\text{scatt}} \propto v^{-4}$) and electric dipole moment ($\sigma_{\text{scatt}} \propto v^{-2}$). In particular, the constraints on the DM charge[2] q read $|q|/e < 1.8 \times 10^{-6} (M/\text{GeV})^{1/2}$. These constraints rely on imprints that would be left at the epoch of hydrogen recombination ($T \simeq 0.3\, \text{eV}$) or later. SQM is charge neutral, thus to understand the relevance of this limits for the scenario considered in this paper we should study the ionization status of SQM at these times. A detailed study is beyond the scope of this paper, however we can gain some insight through a simple quantitative argument, reminiscent of the calculation of the recombination temperature of neutral hydrogen through the Saha equation. To this purpose, we make an educated guess about the energy ΔE_i needed to bring the SQM to

---

[2] See also Singh Sidhu & Starkman (2020) for a discussion of the conditions that allow to apply the constraints in Dvorkin et al. (2014) to macroscopic dark matter candidates such as SQM.

the i-th from the $(i-1)$-th ionized state. The total ionization energy of ordinary atoms is of the order of $E_{ion} \sim (16\,eV) \times Z^{7/3}$, so we can estimate $\Delta E_i \sim dE_{ion}/dZ|_{Z=i} \simeq 30\,eV i^{4/3}$. The high density of photons with respect to SQM should also be taken into account, taking the role played by the larger (yet very small) baryon-to-photon ratio $\eta = n_b/n_\gamma \simeq 6 \times 10^{-10}$ in estimates of the hydrogen recombination temperature. The quantity of relevance would thus be the ratio between the number densities of SQM and photons, $\eta_{SQM} \equiv n_{SQM}/n_\gamma \sim 5(m_P/M)\eta$ where, for the sake of our order-of-magnitude estimates, we have neglected entropy productions taking place before hydrogen recombination. The factor $m_P/M \sim A^{-1}$ is potentially very small for the SQM clumps considered here; however, the dependence of the recombination temperature on η (or η_{SQM}) is only logarithmic. In fact, a direct numerical calculation from the Saha equation shows that, for $\eta_{SQM} = 3 \times 10^{-41}$ (corresponding to $A \sim 10^{32}$) at $T < 10\,eV$, the average ionization state of SQM should be $\lesssim 10$, i.e. each SQM particle behaves as charged dark matter with $|q| \lesssim 10e$. Such a value of the charge is well below the limits reported in Dvorkin et al. (2014).

Finally, we mention the possibility that SQM might absorb standard model particles, in particular protons, neutrons and electrons. This scenario can be constrained by a number of early-time cosmological observables. For example, already Madsen & Riisager (1985) noted that if SQM absorbs protons and neutrons at different rates (as expected in the case of a non-vanishing electrostatic potential) prior to the onset of Big Bang nucleosynthesis (BBN), the predicted abundances of light elements would be altered. Following this line of reasoning, Jacobs et al. (2015) have constrained the reduced cross-section as a function of the electrostatic potential, for generic macroscopic dark matter candidates. For positive values of the potential at the surface of the SQM of the order of $\sim 10\,MeV$, as suggested in Alcock et al. (1986), they find a bound $\sigma_{geom}/M \lesssim 2 \times 10^{-10}\,cm^2\,g^{-1}$. For nuclear-density matter, this corresponds to $M \gtrsim 2\,g$, which is satisfied by the SQM clumps considered here. Caloni et al. (2021) have instead considered the case in which the absorption starts after BBN; this scenario can be constrained by comparing the baryon abundances inferred from light element abundances on one side, and from the CMB anisotropies on the other. The bounds on the reduced cross section, and thus on the SQM mass, in this scenario are however looser than those reported in Jacobs et al. (2015) for absorption taking place before BBN.
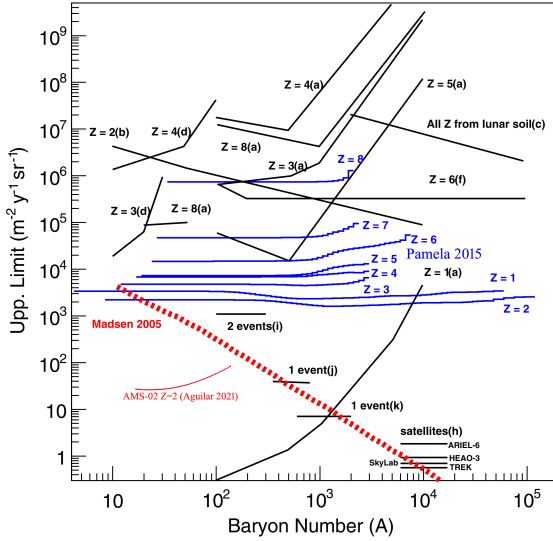
6 SEARCH FOR STRANGELETS

There have been several attempts to search for strangelets or deeply penetrating particles in general. They employ different detection methodologies according to the mass range and the velocity addressed.

- **Light Mass** ($A < 70$)**, non-moving particles**. SQM particles could have accumulated on the Moon or the Earth surface and be detected with mass spectrometers. The Yale Wright Nuclear Structure Laboratory accelerator was employed to search for strangelet particles in lunar soil samples retrieved by the Apollo missions. This kind of ground-based searches has the advantage of using a large amount of matter, providing high statistics, but assumes that strangelets can deposit on the upper layers of lunar or terrestrial soil. In Han et al. (2009) no events for Z = 5-9, and 11 with $42 < A < 70$ were found, with a concentration of strangelets in lunar soil lower than 10^{-16} with respect to normal matter at 95% C.L.

- **Light Mass** ($A \lesssim 10^5$) **, quasi-relativistic particles**. These particles can be directly detected in the flux of cosmic rays as they cross space-borne or balloon-borne detectors. In the 1990 balloon experiment HECRO-81 Saito et al. (1990) reported the observation of two events with $Z \simeq 14$ and an estimated mass $A \simeq 350$. In 1987, the ARIEL-6 satellite (see Fowler et al. (1987)) employing Cherenkov counters, presented an analysis of $Z \geq 34$ finding no SQM candidates in 427 days of data acquisition. The HEAO-3 apparatus (see Binns et al. (1989)), with an exposure of $8 \times 10^{11}\,cm^2\,sr\,s$, did not find any strangelet candidate. Among the passive detectors (similar to the ground mica experiments) the SkyLab experiment (Shirk & Price (1978)), with $1.2\,m^2$ Lexan track detectors, did not find any valid candidate in the superheavy ($Z > 110$) nuclei range. On board the space station Mir, the experiment TREK (Price et al. (1992a)) explored the $Z > 50$ region, also finding no strangelet candidate. In the case of a magnetic spectrometer, strangelets would appear as events having a low deflection due to their high mass/charge (A/Z) ratio, due to the presence of the negative charge of the strange quarks (in case of Z=0 they would be undetectable). BESS balloon-borne detector flights have yielded no candidates for $5 \leq Z \leq 26$ for $A/Z > 5$ Ichimura et al. (1993). Subsequently, data from 2006 to 2009 of the PAMELA space spectrometer were employed to conduct a direct search for SQM within cosmic rays (Adriani et al. 2015a). The spectrometer explored a rigidity range from $1-1000\,GV$ without finding traces of such particles, thereby setting an upper limit on the monochromatic strangelet flux in cosmic rays for particles having charge $1 \leq Z \leq 8$ and baryonic mass $4 \leq A \leq 1.2 \times 10^5$. The AMS-01 Shuttle-Mir flight reported the observation of two events: $Z = 8$, $A = 20$ (3.93 GV) and $Z = 4$, $A = 50$ (5.13 GV), probably due to background, since the following, much longer, AMS-02 mission has found no events and has lowered the limit to the flux of $Z = 2$, yielding the limits represented in Fig. 7.

- **Underground detector, Intermediate mass** $10^{-11}\,g < M \leq 1\,g$. Underground, the MACRO detector placed a limit of 1.1×10^{-14} $cm^{-2}\,sr^{-1}\,s^{-1}$ and $5.5 \times 10^{-15}\,cm^{-2}\,sr^{-1}\,s^{-1}$ in the mass ranges $10^{-11}\,g < m < 0.1\,g$ and $m > 0.1\,g$ respectively Ahlen et al. (1991),

- **High Mass, Meteor-like particle** $10^{-6}\,g \lesssim M \lesssim 10^4\,g$. Since strangelets can be rather massive, their presence can be inferred through the seismic activity they can potentially induce on the Moon, as suggested in Banerdt et al. (2006). According to Nakamura & Frohlich (2006), most of a rare class of lunar seismic events detected by the Apollo lunar seismic network occurred when the Moon faced a specific direction of the celestial sphere, suggesting that they may be caused by objects of extra-solar origin. Strangelets can also give a meteor-like signal as they burn in the atmosphere, with tracks that are either longer and/or faster than those of conventional meteors. Pi in the SKY, searching for fast meteors in the sky (Piotrowski et al. 2020), yielded a limit close to the dark matter constraint. The DIMS experiment is currently searching for these events from the ground, using two cameras for stereoscopic view of meteors and determination of their trajectory (Abe et al. 2021). Similarly, Mini-EUSO is searching for these events from the ISS (Adams et al. 2015; Bacholle et al. 2021) with a wider field. Another detector, SQM-ISS, aiming for direct detection of SQM, is being designed to be placed on the ISS in the next years. In this case, the idea is to use a local compact detector composed of a stack of scintillators (to detect ionization by passing particles) and a stack of metal plates (to read the vibration caused by the passage of particles) coupled to a time-of-flight system capable of measuring the speed of the particle. Strangelets or similar particles are expected to move through the detector unaffected by the ISS hull, at speeds consistent with the galactic orbital velocity of $\sim 220\,km/s$ or lower.

Figure 7. Strangelet flux integral upper limits vs mass. The dotted line represents the dark matter constraint, assuming that all dark matter in the galaxy is composed by a single mass particle (Madsen 1988; Madsen et al. 1986). The solid black lines represent experimental limits for strangelets converted into flux limits. The curves labeled (a) (Hemmick et al. 1990), (b) (Mueller et al. 2004), (d) (Klein, Midleton & Stephens Klein et al.), (e) (Middleton et al. 1979), and (f) (Turkevich et al. 1984) come from relic searches in terrestrial material. The curve labeled (c) (Isaac et al. 1998) comes from searches which bombard materials with slow-moving heavy ions. The curves labeled with (h) (Fowler et al. 1987; Binns et al. 1989; Shirk & Price 1978; Price et al. 1992b) represent satellite-based searches, obtained from the exposure of the single experiments assuming Poissonian statistics. The curves labeled with (i) (Saito et al. 1990), (j) (Ichimura et al. 1993), and (k) (Price et al. 1978) represent detection of events consistent with strangelet signals by balloon-borne cosmic-ray detectors. The blue curves are PAMELA measurements for nuclei up to $Z = 8$ Adriani et al. (2015b), the red one is the AMS-02 measurement for $Z = 2$ Aguilar et al. (2021).

- **High-Mass Asteroid-size celestial bodies with $M \lesssim 10^{21}$ g,** such as Polyhymnia and Ludmilla (Carry (2012)) both with mass densities of about 75 g/cm^3 have been proposed as being constituted of either ultra-heavy (Z>120) nuclei or SQM. Although more prosaically their anomalous density is due to uncertainties in the mass determination related to the difficulty of orbital perturbations, a systematic search for anomalous density asteroids could place a limit in this mass range.

With a more refined theoretical framework to establish the possible sizes and eventually charges of strangelets, future experiments could be designed more effectively to search for these elusive particles. In particular, the space-based search, as opposed to ground-based one, can potentially identify strangelets without necessitating assumptions about their interaction with the Earth's atmosphere.

7 CONCLUSIONS

In this article we have revisited the possibility that dark matter is made of clusters of up, down and strange quarks, as suggested by Witten (1984). We have shown that it is at least conceptually possible to formulate a scheme, leading to the formation of those objects in the Early Universe, without assuming the existence of a first-order phase transition associated with confinement. The recent experimen-

tal results, showing that nuclei can form at high temperatures in ultra-relativistic heavy ion collisions, support the claim that clusterization does not need to be associated with a first-order transition.

We have investigated a simple scheme, based on the formation of quark clusters at the hadronization temperature, which later partially evaporate, and we have shown that these objects can satisfy all the astrophysical and cosmological constraints on dark matter.

We have shown that SQM is not strongly self-interacting and that it can be considered charge neutral. On the other hand, it has a finite inelastic cross section with itself and with ordinary matter, but the implications of this property for the evolution of galaxies still need to be worked out.

REFERENCES

Abe S., et al., 2021, PoS, ICRC2021, 554
Adam J., et al., 2016, Phys. Lett. B, 754, 360
Adams J. H., et al., 2015, Experimental Astronomy, 40, 253
Adriani O., et al., 2015a, Phys. Rev. Lett., 115, 111101
Adriani O., et al., 2015b, Phys. Rev. Lett., 115, 111101
Afzal A., et al., 2023, The Astrophysical Journal Letters, 951, L11
Aguilar M., et al., 2021, Physics Reports, 894, 1
Ahlen S., et al., 1991, Nuclear Physics B - Proceedings Supplements, 24, 191
Alba P., Sarti V. M., Noronha-Hostler J., Parotto P., Portillo-Vazquez I., Ratti C., Stafford J. M., 2020, Phys. Rev. C, 101, 054905
Alberico W. M., Drago A., Ratti C., 2002, Nucl. Phys. A, 706, 143
Alcock C., Farhi E., 1985, Phys. Rev. D, 32, 1273
Alcock C., Farhi E., Olinto A., 1986, Astrophys. J., 310, 261
Alford M., Reddy S., 2003, Phys. Rev. D, 67, 074024
Alford M. G., Schmitt A., Rajagopal K., Schäfer T., 2008, Rev. Mod. Phys., 80, 1455
Alford M. G., Harris S. P., Sachdeva P. S., 2017, Astrophys. J., 847, 109
Anglani R., Casalbuoni R., Ciminale M., Ippolito N., Gatto R., Mannarelli M., Ruggieri M., 2014, Rev. Mod. Phys., 86, 509
Aoki Y., Endrodi G., Fodor Z., Katz S. D., Szabo K. K., 2006, Nature, 443, 675
Bacholle S., et al., 2021, The Astrophysical Journal Supplement Series, 253, 36
Banerdt W. B., Chui T., Herrin E. T., Rosenbaum D., Teplitz V. L., 2006, Advances in Space Research, 37, 1889
Barnacka A., Glicenstein J.-F., Moderski R., 2012, Physical Review D, 86
Bauswein A., Oechslin R., Janka H. T., 2010, Phys. Rev. D, 81, 024012
Bellwied R., Borsanyi S., Fodor Z., Katz S. D., Ratti C., 2013, Phys. Rev. Lett., 111, 202302
Bellwied R., et al., 2021, Phys. Rev. D, 104, 094508
Bertolucci S., Zioutas K., Hofmann S., Maroudas M., 2017, Physics of the Dark Universe, 17, 13
Binns W. R., et al., 1989, ApJ, 346, 997
Braun-Munzinger P., Dönigus B., 2019, Nucl. Phys. A, 987, 144
Buballa M., 2005, Phys. Rept., 407, 205
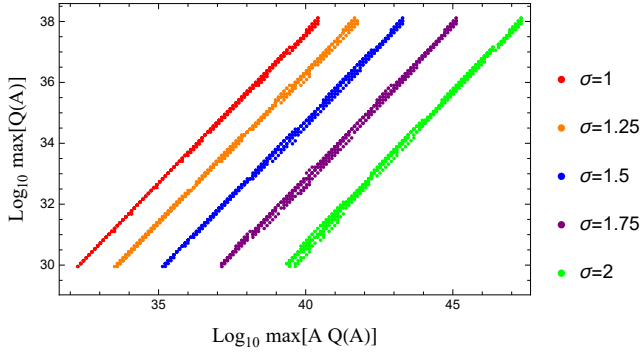Bucciantini N., Drago A., Pagliara G., Traversi S., Bauswein A., 2022, Phys. Rev. D, 106, 103032

Bullock J. S., Boylan-Kolchin M., 2017, Ann. Rev. Astron. Astrophys., 55, 343

Burdin S., Fairbairn M., Mermod P., Milstead D., Pinfold J., Sloan T., Taylor W., 2015, Phys. Rept., 582, 1

Caloni L., Gerbino M., Lattanzi M., 2021, JCAP, 07, 027

Carlson E. D., Machacek M. E., Hall L. J., 1992, Astrophys. J., 398, 43

Carry B., 2012, Planet. Space Sci., 73, 98

Chodos A., Jaffe R. L., Johnson K., Thorn C. B., Weisskopf V. F., 1974, Physical Review D, 9, 3471

Christensen K., Moloney N., 2005, Complexity and Criticality. Advanced physics texts, Imperial College Press, https://books.google.it/books?id=bAIM1_EoQu0C

Davis S., Smith A., 1973, Kolloid-Zeitschrift und Zeitschrift für Polymere

Di Clemente F., Mannarelli M., Tonelli F., 2020, Phys. Rev. D, 101, 103003

Di Clemente F., Drago A., Pagliara G., 2022, arXiv e-prints, p. arXiv:2211.07485

Di Clemente F., Drago A., Char P., Pagliara G., 2023, Astron. Astrophys., 678, L1

Di Salvo T., Sanna A., Burderi L., Papitto A., Iaria R., Gambino A. F., Riggio A., 2019, Mon. Not. Roy. Astron. Soc., 483, 767

Dolgov A. D., Dubovsky S. L., Rubtsov G. I., Tkachev I. I., 2013, Phys. Rev. D, 88, 117701

Dolgov A., Kuranov A., Mitichkin N., Porey S., Postnov K., Sazhina O., Simkin I., 2020, Journal of Cosmology and Astroparticle Physics, 2020, 017–017

Dondi N., Drago A., Pagliara G., 2017, EPJ Web of Conferences, 137, 09004

Doroshenko V., Suleimanov V., Puehlhofer G., Santangelo A., 2022, Nature Astronomy

Drago A., Lavagno A., 2001, Phys. Lett. B, 511, 229

Drago A., Pagliara G., 2016, Eur. Phys. J. A, 52, 41

Drago A., Lavagno A., Pagliara G., 2004, Phys. Rev. D, 69, 057505

Drago A., Lavagno A., Parenti I., 2007, Astrophys. J., 659, 1519

Drago A., Lavagno A., Pagliara G., 2014a, Phys. Rev. D, 89, 043014

Drago A., Lavagno A., Pagliara G., Pigato D., 2014b, Phys. Rev. C, 90, 065809

Drago A., Lavagno A., Pagliara G., Pigato D., 2016, Eur. Phys. J. A, 52, 40

Dvorkin C., Blum K., Kamionkowski M., 2014, Phys. Rev. D, 89, 023519

Farhi E., Jaffe R. L., 1984, Phys. Rev. D, 30, 2379

Farrar G. R., 2022, A Stable Sexaquark: Overview and Discovery Strategies (arXiv:2201.01334)

Flor F. A., Olinger G., Bellwied R., 2021, Phys. Lett. B, 814, 136098

Fowler P. H., Walker R. N. F., Masheder M. R. W., Moses R. T., Worley A., Gay A. M., 1987, ApJ, 314, 739

Freedman B., McLerran L. D., 1978, Phys. Rev. D, 17, 1109

Gao F., Oldengott I. M., 2022, Phys. Rev. Lett., 128, 131301

Glendenning N. K., Kettner C., Weber F., 1995a, Phys. Rev. Lett., 74, 3519

Glendenning N. K., Kettner C., Weber F., 1995b, Astrophys. J., 450, 253

Haensel P., Zdunik J. L., Schaefer R., 1986, A&A, 160, 121

Han K., et al., 2009, Phys. Rev. Lett., 103, 092302

Hemmick T. K., et al., 1990, Phys. Rev. D, 41, 2074

Herrin E. T., Rosenbaum D. C., Teplitz V. L., 2006, Phys. Rev. D, 73, 043511

Ichimura M., et al., 1993, Il Nuovo Cimento A (1965-1970), 106, 843

Isaac M. C. P., et al., 1998, Phys. Rev. Lett., 81, 2416

Jacobs D. M., Starkman G. D., Lynn B. W., 2015, Mon. Not. Roy. Astron. Soc., 450, 3418

Jaffe R. L., 1977, Phys. Rev. Lett., 38, 195

Katz A., Kopp J., Sibiryakov S., Xue W., 2018, JCAP, 12, 005

Kettner C., Weber F., Weigel M. K., Glendenning N. K., 1995, Phys. Rev. D, 51, 1440

Klahn T., Fischer T., 2015, Astrophys. J., 810, 134

Klein J., Midleton R., Stephens W. E., , Argonne National Laboratory Report No. ANL/PHY-81-1, 1981

Kurban A., Huang Y.-F., Geng J.-J., Zong H.-S., 2022, Phys. Lett. B, 832, 137204

Kurkela A., Romatschke P., Vuorinen A., 2010, Phys. Rev. D, 81, 105021

Letessier J., Rafelski J., 2002, Hadrons and Quark–Gluon Plasma. Oxford University Press, doi:10.1017/9781009290753

Madsen J., 1988, Phys. Rev. Lett., 61, 2909

Madsen J., Riisager K., 1985, Phys. Lett. B, 158, 208

Madsen J., Heiselberg H., Riisager K., 1986, Phys. Rev. D, 34, 2947

Martens G., Greiner C., Leupold S., Mosel U., 2006, Phys. Rev. D, 73, 096004

Middleton R., Zurmühle R. W., Klein J., Kollarits R. V., 1979, Phys. Rev. Lett., 43, 429

Mueller P., Wang L.-B., Holt R. J., Lu Z.-T., O'Connor T. P., Schiffer J. P., 2004, Phys. Rev. Lett., 92, 022501

Nakamura Y., Frohlich C., 2006, in Mackwell S., Stansbery E., eds, 37th Annual Lunar and Planetary Science Conference. Lunar and Planetary Science Conference. p. 1048

Navarro J. F., Frenk C. S., White S. D. M., 1997, Astrophys. J., 490, 493

Nesti F., Salucci P., 2013, Journal of Cosmology and Astroparticle Physics, 2013, 016–016

Pereira J. P., Flores C. V., Lugones G., 2018, Astrophys. J., 860, 12

Piotrowski L. W., Małek K., Mankiewicz L., Sokołowski M., Wrochna G., Zadrożny A., Żarnecki A. F., 2020, Phys. Rev. Lett., 125, 091101

Pollack J., Spergel D. N., Steinhardt P. J., 2015, Astrophys. J., 804, 131

Price P. B., Salamon M. H., 1986, Phys. Rev. Lett., 56, 1226

Price P. B., Shirk E. K., Osborne W. Z., Pinsky L. S., 1978, Phys. Rev. D, 18, 1382

Price P. B., et al., 1992b, Ap&SS, 197, 121

Price P. B., et al., 1992a, Astrophysics and Space Science, 197, 121

Saito T., Hatano Y., Fukada Y., Oda H., 1990, Phys. Rev. Lett., 65, 2094

Shahrbaf M., Blaschke D., Typel S., Farrar G. R., Alvarez-Castillo D. E., 2022, Phys. Rev. D, 105, 103005

Shirk E. K., Price P. B., 1978, ApJ, 220, 719

Shuryak E., Torres-Rincon J. M., 2020, Phys. Rev. C, 101, 034914

Singh Sidhu J., Starkman G. D., 2020, Phys. Rev. D, 101, 083503

Spergel D. N., Steinhardt P. J., 2000, Phys. Rev. Lett., 84, 3760

Suwa Y., Yoshida T., Shibata M., Umeda H., Takahashi K., 2018, Mon. Not. Roy. Astron. Soc., 481, 3305

Turkevich A., Wielgoz K., Economou T. E., 1984, Phys. Rev. D, 30, 1876

Vartanyan Y. L., Hajyan G. S., Grigoryan A. K., Sarkisyan T. R., 2009, Astrophysics, 52, 300

Vartanyan Y. L., Hajyan G. S., Grigoryan A. K., Sarkisyan T. R., 2012, Astrophysics, 55, 98

Watkins L. L., van der Marel R. P., Sohn S. T., Wyn Evans N., 2019, The Astrophysical Journal, 873, 118

Watts A. L., Reddy S., 2007, Mon. Not. Roy. Astron. Soc., 379, L63

Wiktorowicz G., Drago A., Pagliara G., Popov S. B., 2017, Astrophys. J., 846, 163

Witten E., 1984, Phys. Rev. D, 30, 272

Zhitnitsky A. R., 2003, Journal of Cosmology and Astroparticle Physics, 2003, 010–010

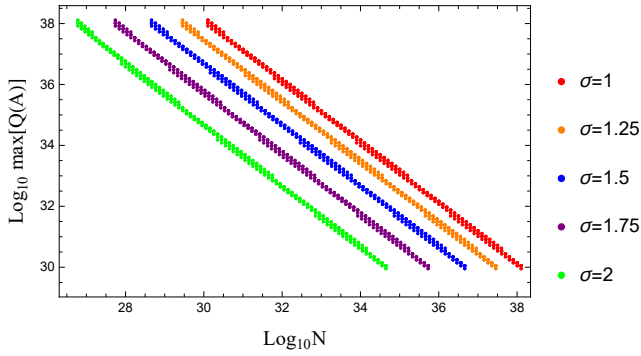## APPENDIX A: EXPLORATION OF THE PARAMETER SPACE

In order to produce the distributions in Fig. 3 we systematically explored the parameter space. To generate the series of plots presented in Fig. A1, Fig. A2, Fig. A3, Fig. A4, and Fig. A5, we employed a detailed evaporation routine. This routine was executed over a range of parameters: the initial central value of the distribution $\mu_{\max} \in [30, 38]$, the standard deviation $\sigma \in [1, 2]$, and $\log_{10}\beta \in [-5, -6]$ for $T_{\text{evap}} = 150$ MeV. Moreover, we used the range $\log_{10}\beta \in [-3, -4]$ for $T_{\text{evap}} = 50$ MeV, to show a strong correlation between the β parameter and the evaporation temperature T_{evap} (see subsection 3.1).

The selection of these parameter ranges was informed by preliminary investigations, which explored a broader parameter space. However, simulations conducted outside those ranges failed to satisfy all the constraints delineated in Section 2. Consequently, to ensure the relevance with respect to the established observational constraints, our analysis was restricted to these specific ranges.

Fig. A1 shows a linear correlation between the log of the maximum

Figure A1. Correlation between the maximum mass and the maximum size of the final distribution, for different values of σ and for $\log_{10}\beta$ varying from -5 to -6.
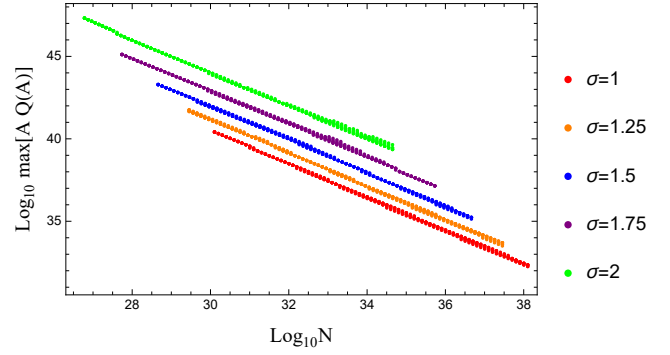

Figure A2. Correlation between the final number of strangelets and the maximum size of the final distribution, for different values of σ and for $\log_{10}\beta$ varying from -5 to -6.

Figure A3. Correlation between the number of strangelets and the maximum mass, for different values of β and for σ varying from 1 to 2.

Figure A4. Correlation between the maximum mass and the DMR, varying β for $T_{\text{evap}} = 150$ MeV

Figure A5. Correlation between the maximum mass and the DMR, varying β for $T_{\text{evap}} = 50$ MeV

of the mass distribution $AQ(A)$, LMAQ, and the log of the maximum of the number distribution $Q(A)$, LMQ. This correlation is observed when the parameters σ (of the pre-evaporation distribution $P(A)$) and β (from Eq. 12) are held constant.
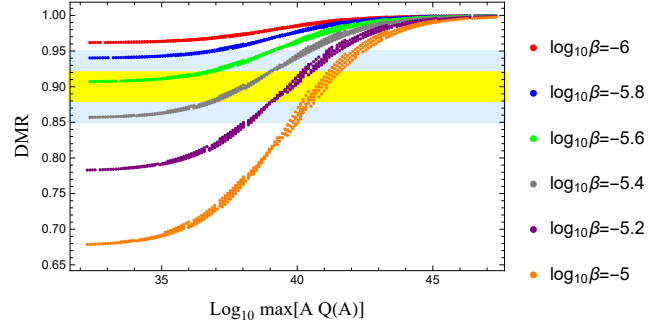
A similar linear correlation exists, for fixed values of σ and β, between the log of the total number of strangelets after evaporation and LMQ (Fig. A2) or LMAQ (Fig. A3).

A non-linear correlation is identified instead in Fig. A4 and Fig. A5, for various values of $\log_{10}\beta$, between the dark matter ratio (DMR) and LMAQ. This relationship suggests that, to achieve the correct DMR, we have to significantly suppress the evaporation rate. It is important to note that, by choosing a lower value of T_{evap}, the suppression of the evaporation rate can be less dramatic. In other words, the role played by β and T_{evap} is very similar.
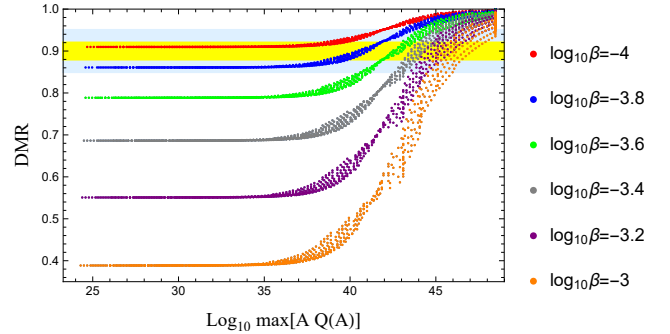
This paper has been typeset from a TEX/LATEX file prepared by the author.